Research Article

Algae 2024, 39(3): 177-186
https://doi.org/10.4490/algae.2024.39.8.26
Open Access

Quantitative detection of *Pythium porphyrae* and *Pythium chondricola* (Oomycota), the causative agents of red rot disease in *Pyropia* farms in China

Jie Liu[1,2], Sudong Xia[1,*], Huichao Yang[2,3], Zhaolan Mo[2,3,4], Jie Li[2,3] and Yongwei Yan[2,3,*]

[1]*Tianjin Key Lab of Aqua-Ecology and Aquaculture, Department of Fishery Science, Tianjin Agricultural University, Tianjin 300384, China*
[2]*State Key Laboratory of Mariculture Biobreeding and Sustainable Goods, Yellow Sea Fisheries Research Institute, Chinese Academy of Fishery Sciences, Qingdao 266071, China*
[3]*Laboratory for Marine Fisheries Science and Food Production Processes, Laoshan Laboratory, Qingdao 266237, China*
[4]*Key Laboratory of Tropical Aquatic Germplasm of Hainan Province, Sanya Oceanographic Institution, Ocean University of China, Sanya 572000, China*

Red rot disease is one of the notorious algal diseases that threaten the cultivation of *Pyropia* in China, and two *Pythium* pathogens, i.e., *Pythium porphyrae* and *P. chondricola*, have been reported as causative agents. To monitor the pathogens, a fluorescent quantitative polymerase chain reaction (PCR) method was developed to quantitatively detect their abundance. Using overlapping PCR and pathogen-specific primer pairs, two pathogen-specific fragments were concatenated to construct an internal standard plasmid, which was used for quantification. For zoospores of known numbers, the results showed that this method can detect as less as 100 and 10 zoospores mL^{-1} in a 200 mL solution for *P. porphyrae* and *P. chondricola*, respectively. Using monthly collected seawater at 10 sites in Haizhou Bay, a typical aquaculture farm in China, a significantly higher temperature and a significantly lower salinity were determined in December 2021. *P. porphyrae* was determined to be more abundant than *P. chondricola*, though with similar temporal distribution patterns from December 2021 to February 2022. When a red rot disease occurred in December 2021, the two pathogens were significantly more abundant at two infected sub-sites than the uninfected sub-site within both seawater and sediment, though they were all significantly more enriched in sediment than in seawater. The present method provides the capability to quantify and compare the abundance of two pathogens and also has the potential to forecast the occurrence of red rot disease, which is of much significance in managing and controlling the disease.

Keywords: *Pyropia*; *Pythium chondricola*; *Pythium porphyrae*; quantification; red rot disease

INTRODUCTION

Pyropia spp. (Bangiales, Rhodophyta), described as *Pyropia sensu lato* recently (Yang et al. 2020), have been cultivated in East Asia for a long time, including China, Korea, and Japan. With the continuous development of the aquaculture industry, the production volume and culturing area are increasing, which led to disease problems becoming more and more prominent. Bacteria, viruses, fungi, and other eukaryotes have all been impli-

Received May 27, 2024, **Accepted** August 26, 2024
***Corresponding Author**
E-mail: yanyw@ysfri.ac.cn (Y. Yan)
Tel: +86-532-85823062, Fax: +86-532-8581514
E-mail: xsd20022003@126.com (S. Xia)
Tel: +86-139-20435896

cated in a growing list of algal disease pathogens (Gachon et al. 2010, Ward et al. 2019, Behera et al. 2022). In China, disease outbreaks can lead to a regional loss of *Pyropia* reaching 25–30% (Gachon et al. 2010). Among these, red rot disease is one of the most disastrous diseases for *Pyropia* cultivation in China, which can cause serious yield and economic losses once occurred. For example, in 2008, it is reported a reduction of 84% in *Pyropia haitanensis* yield in the city of Fuding, Fujian province, China (Lai 2009). In January 2018, the reduction rate of *Pyropia yezoensis* was estimated to be 50% (approximately over 7,000 hectares) in Haizhou Bay, Jiangsu Province, China (Yan et al. 2019).

Despite a report of fungus pathogen *Alternaria* sp. (Mo et al. 2016), oomycetic pathogens in genus *Pythium*, i.e., *Pythium porphyrae* and *P. chondricola*, are typically reported to be the causative agents of red rot disease (Takahashi et al. 1977, Kazama 1979, Ding and Ma 2005, Lee et al. 2015, Qiu et al. 2019). The oomycetic pathogens can be spread by zoospores that are released into seawater, which will then attach to algae thalli, germinate, grow hyphae, and finally kill the algae within a few days along with the release of a large number of new zoospores (Park et al. 2001). To control the disease, certain methods have been adopted, such as air-dry, frozen-net around -20°C, acid-washing, and the newly developed net-washing with calcium propionate (Kim et al. 2014, Wen et al. 2023). Recently, disease-resistant algal strain (Lee et al. 2015) and biocontrol bacteria (Weng et al. 2024) have been developed, and provide a promising future for disease control. Despite all these attempts, more efforts are still required, with environmental issues being one of the major concerns (Wen et al. 2023). Besides, most of the control methods are typically effective when implemented at the early infection stage (Wen et al. 2023, Weng et al. 2024). Given such observation, it is necessary to evaluate aquaculture environments, hence the prediction of disease risk.

The quantification of pathogen abundance notably zoospore concentrations may be one of the effective approaches to forecasting disease. For this purpose, researchers have established a series of methods to monitor *P. porphyrae*. For example, immunological detection using monoclonal antibodies (Amano et al. 1995, 1996), competitive polymerase chain reaction (PCR) (Park et al. 2001), quantitative PCR (qPCR) method (Satoshi 2016), and restriction fragment length polymorphism (RFLP) (Lee and Lee 2022). The immunological method is suitable for the detection of attached and germinated zoospores rather than non-germinated zoospores (Park et al. 2001), thus unable to forecast disease prior to infection. In comparison, PCR-based methods are usually proved to be specific and efficient for the detection of zoospores. Using competitive PCR, for example, it is proved that approximately 10 and 100 zoospores can infect thalli within three to four days, and more zoospores lead to more infection in both the laboratory and cultivation areas (Park et al. 2006). Recently, the developed PCR-RFLP is capable of detecting both *P. porphyrae* and *P. chondricola*, which provides an efficient method for the long-term detection of *Pythium* pathogens in aquaculture farms.

Given limited methods for the quantitative detection of both *Pythium* pathogens, the present study aimed to develop a method to quantify the abundance of *P. porphyrae* and *P. chondricola*, which was then used to quantify them in different types of environmental samples.

MATERIALS AND METHODS

Cultivation of *Pythium* strains and zoospore induction

Pythium strains used in the present study were purchased from the NITE Biological Resource Center (NBRC), Department of Biotechnology, National Institute of Technology and Evaluation (NITE), Japan, China General Microbiological Culture Collection Center (CGMCC), or isolated and maintained by our lab (Supplementary Table S1). Strains affiliated with *P. porphyrae* and *P. chondricola* were maintained on corn meal yeast extract seawater agar (CMYSWA) at the appropriate temperature in the dark as referred by NBRC. Plugs of CMYSWA containing the edge of the *Pythium* growth circle were inoculated into a 50% seawater glucose glutamate liquid medium (Fujita and Zenitani 1977) and incubated at the appropriate temperature. After 15 days, the mycelia mats were collected by filtration and used for total genomic DNA extraction.

Pythium zoospore suspension was induced and prepared according to a previously reported method (Addepalli and Fujita 2002). The concentrations of zoospores were determined using light microscopy with a haemacytometer. All counts were performed in five replicates.

Primers and construction of internal standard plasmid

Primers used in the present study are listed in Table 1. Primer pairs specific to the amplification of *P. porphyrae* (P-for and P-rev) and *P. chondricola* (C-for and C-rev)

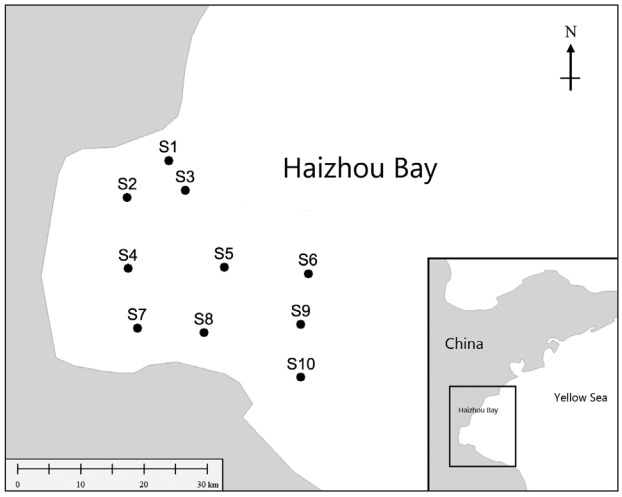

Fig. 1. Distribution of sampling sites in Haizhou Bay, the cultivation farm of *Pyropia yezoensis* in China.

were direct applications of a China patent (No. ZL 202011483053.5), and more details about the methodology are in the Supplementary Method S1. An internal standard plasmid containing two pathogen-specific fragments was constructed. Briefly, the two pathogen-specific fragments were separately amplified using the total genomic DNA of two pathogen strains, which was extracted from mycelia mats using an E.Z.N.A. HP Fungal DNA Kit (Omega Bio-tek, Norcross, GA, USA). The two amplified fragments were recycled using a GEL/PCR Purification Mini Kit (Solarbio, Beijing, China), which were then co-amplified and concatenated using an overlapping PCR (Heckman and Pease 2007), and a little modification was made (Supplementary Fig. S1A). A primer designated as PC-m-for (Table 1) was used in the overlapping PCR, which was designed based on reverse-complemented P-rev and the original C-for (Supplementary Fig. S1A). The concatenated fragment of the predicted size was recycled using the GEL/PCR Purification Mini Kit. The resulting product was inserted into the pCloneEZ-NRS-TA vector, and the internal standard plasmid PC-m was constructed. PC-m was transformed into *Escherichia coli* DH10β, and positive clones were then selected and checked using PCR amplification with M13F and M13R (Table 1). Positive clones were cultivated in Luria-Berani medium supplemented with 100 μg mL^{-1} ampicillin, and the plasmid was extracted using an E.Z.N.A. Plasmid Mini Kit (Omega Bio-tek). The plasmid was dissolved in TE buffer and quantified using Nanodrop 2000 (Thermo Scientific, Waltham, MA, USA). The copy number of the internal standard plasmid was calculated as follows:

$$c\ (\text{copies}) = \frac{6.02 \times 10^{23}\ (\text{copies mol}^{-1}) \times m\ (\text{g})}{1\ (\text{bp}) \times 660\ (\text{g mol}^{-1}\ \text{bp}^{-1})}$$

In the equation, "c" indicates the copy number of the standard plasmid, "m" indicates the amount of the plasmid, and "l" indicates the length of the plasmid.

Collections of zoospores and environmental samples

The quantified plasmid PC-m was diluted in ten-fold series using EASY Dilution (Takara, Dalian, China), which was then used for qPCR to construct standard curves. To estimate zoospore concentrations using pathogen abundance, zoospores of each pathogen were diluted in a ten-fold series using 10 mM $CaCl_2$ solution, and then approximately 200 mL suspension was filtered using a mixed cellulose membrane (0.22 μm pore size) for each dilution. The total DNA of zoospores was extracted using the E.Z.N.A. HP Fungal DNA Kit, which was then used for pathogen quantification.

Environmental samples were collected from 10 sites in Haizhou Bay, a typical *P. yezoensis* cultivation area in Jiangsu province of China. The sampling sites are shown in Fig. 1, and sample types are supplied in Supplementary Table S2. At each site, four replicate seawater samples (500 mL per replicate) were collected. On December 23, 2021, an additional sampling for seawater and sediment was performed at three sub-sites around S9 due to an onset

Table 1. Primer sequences used in the present study

Target	Primers	Primers (5′-3′)	Product length (bp)
Pythium porphyrae	P-for	CCTACAGCAATCCACGAGACTC	893
	P-rev	TGCCGTAGAGAAGAACACAGAGA	
P. chondricola	C-for	CGGACACGAAGACGACGCTAT	339
Overlapping primer	C-rev	CGACTACGACTACGACTACGACTAT	
	PC-m-for	TCTCTGTGTTCTTCTCTACGGCACGGACACGAAGACGACGCTAT	1,232
Inserted fragment	M13F	TGTAAAACGACGGCCAGT	1,374
	M13R	AGGAAACAGCTATGACC	

of red rot disease, which included the original S9 site and two infected sub-sites (S9-1 and S9-2). For each sub-site, triplicate samples were collected. Seawater temperature, pH, salinity, and dissolved oxygen (DO) were recorded in situ with a water-quality sampling and monitoring meter (YSI Life Sciences, Yellow Springs, OH, USA) at a depth of approximately 50 cm. For each seawater sample, approximately 200 mL seawater was filtered using mixed cellulose membrane (0.22 μm pore size) for DNA extraction as aforementioned, and the remaining was used to measure concentrations of NO_3^--N, $PO4_3^-$-P, NO_2^--N, NH_4^+-N, and SiO_3^{2-}-Si using a nutrient analyzer (SINOHLK, Qingdao, China). Regarding sediment samples, the total DNA was extracted using a DNeasy Powersoil Kit (Qiagen, Valencia, CA, USA) according to the manufacturer's instructions.

Quantification of pathogen abundance

All samples were amplified using a 20-μL reaction system, which contains 10 μL SYBR Green Realtime PCR Master Mix (2×) (Toyobo, Osaka, Japan), 1 μL (10 μM) forward primer, 1 μL (10 μM) reverse primer, 7 μL RNase/DNase-free water (Tiangen, Beijing, China), and 1 μL diluted template DNA. All qPCR tubes were placed in a CFX Connect thermal cycler (Bio-Rad, Hercules, CA, USA). The program used for *P. porphyrae* quantification was as follows: initial denaturation at 95°C for 1 min, 40 cycles of 95°C for 15 s, 55°C for 15 s, and 72°C for 40 s, with the fluorescence then being read. For the quantification of *P. chondricola*, the extension in each cycle was revised to 72°C for 25 s. At the end of the program, to verify the primer specificity, melting curve analysis was performed from 65 to 95°C at a rate ramp of 0.1°C s^{-1} and the fluorescence was read every 5 s. Nuclease-free water was used as a negative control. Three or four technical replicates were used for each sample.

A standard curve for each pathogen was constructed using the internal standard plasmid with ten-fold serial dilutions, and a fitting linear curve was determined using C_t values versus the log of the plasmid copy number. The amplification efficiency (E) was calculated as $E = 10^{-1/\text{slope}} - 1$ (Vandesompele et al. 2002), within which the slope indicates the slope of the fitting curve. For zoospores of known numbers and environmental samples, abundance determination was performed based on the observed C_t values and the fitting curve for each pathogen. To compare pathogen abundance, a two-tailed t-test was used for two groups, and a one-way analysis of variance (ANOVA) with Tukey's *post-hoc* test was used for three groups.

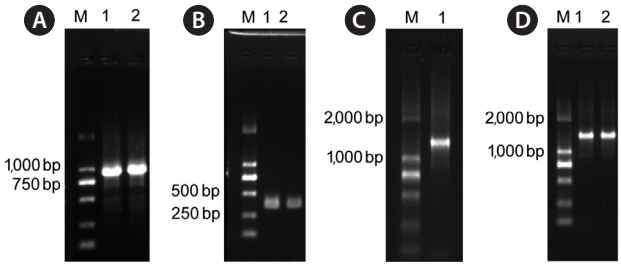

Fig. 2. Gel electrophoresis of polymerase chain reaction products. (A) Amplification of *Pythium porphyrae*-specific fragment. M, DL2000 maker; lanes 1 and 2, amplified fragments. (B) Amplification of *P. chondricola*-specific fragment. M, DL2000 maker; lanes 1 and 2, amplified fragments. (C) Concatenated fragment. M, DL2000 maker; lane 1, amplified fragment. (D) Positive clones verified using M13F and M13R. M, DL2000 maker; lanes 1 and 2, amplified clones.

RESULTS

Construction of internal standard plasmid

Phylogenetic analysis was performed using *cox*1 and *cox*2 to verify the taxonomic information of *Pythium* strains (Supplementary Fig. S2). According to the results, strain NBRC No. 30800 was affiliated with *P. porphyrae* strain NBRC No. 33126. The isolated strains maintained in our lab were all affiliated with *P. chondricola* strain CBS 203.85. Furthermore, the *Pythium* strains NBRC No. 33253 and NBRC No. 100633 were also determined to be affiliated with *P. chondricola*. For the specificity test, the *P. porphyrae*-related fragment can be amplified from NBRC No. 33126 and NBRC No. 30800, while the *P. chondricola*-related fragment can be amplified from NBRC No. 33253 and NBRC No. 100633 in addition to our isolated strains (China patent: No. ZL 202011483053.5). Both fragments cannot be amplified from other microbes listed in Supplementary Table S1.

Specific fragments were amplified from *P. porphyrae* NBRC No. 30800 and *P. chondricola* NBRC No. 33253, respectively. As shown in Fig. 2, the pathogen-specific primer pairs amplified gene fragments approximately the same length as predicted for both *P. porphyrae* (Fig. 2A) and *P. chondricola* (Fig. 2B). After overlapping PCR, a PCR fragment larger than 1,000 bp was generated (Fig. 2C). After gene cloning, positive clones were selected and sequenced (Fig. 2D). As a result, the recombinant fragment inserted into the vector is approximately 1,232 bp, which is the same as the summed length of the fragments amplified from *P. porphyrae* and *P. chondricola* (Supplementary Fig. S1B).

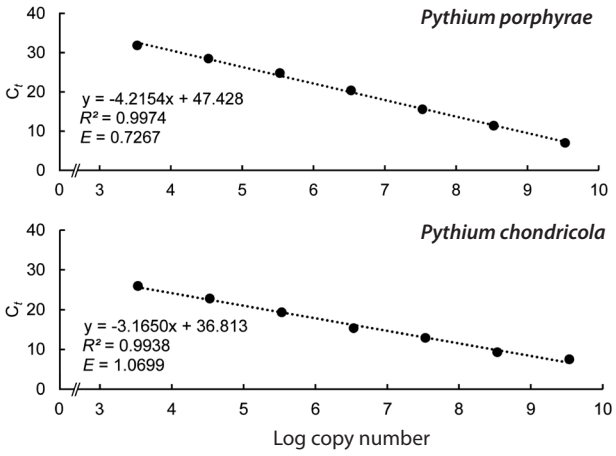

Fig. 3. Construction of standard curves for *Pythium porphyrae* and *P. chondricola*, respectively.

Construction of standard curves

Ten-fold serial dilutions resulted in 10^9, 10^8, 10^7, 10^6, 10^5, 10^4, and 10^3 copies μL^{-1} of the plasmid (Supplementary Fig. S3A & C). By using them as templates, the constructed standard curves for *P. porphyrae* and *P. chondricola* are shown in Fig. 3. The obtained R^2 for the two curves were both larger than 0.99, which indicates good dilution and linearization. Furthermore, the melting curves for *P. porphyrae* and *P. chondricola* peaked at approximately 85.5°C (Supplementary Fig. S3B) and 91°C (Supplementary Fig. S3D), respectively, indicating specific amplification for the two pathogens. The amplification efficiency was estimated to be 0.73 for *P. porphyrae* (Fig. 3), while that for *P. chondricola* was approximately 1.07 (Fig. 3).

Quantification of pathogen abundance using zoospores

The results are shown in Table 2. When concentrations range from 1.4×10^4 to 1.4×10^6 zoospores mL^{-1}, the abundance of *P. porphyrae* was determined to be $(5.86 \pm 0.35) \times 10^0$–$(2.34 \pm 0.24) \times 10^2$ copies mL^{-1}. When the concentrations decreased from 1.4×10^2 to 1.4×10^3 zoospores mL^{-1}, the abundance was estimated to be $(4.62 \pm 0.82) \times 10^{-1}$–$(1.58 \pm 0.03) \times 10^0$ copies mL^{-1}. No detection for 1.4×10^1 zoospores mL^{-1}. Regarding *P. chondricola*, the determined abundance was approximately one order of magnitude lower than zoospore concentrations. For approximately the same zoospore concentrations, i.e., 10^2, 10^3, and 10^4 zoospores mL^{-1}, the estimated abundance for the two pathogens was significantly different, with the difference between *P. porphyrae* and *P. chondricola* approximately two (for 10^2 and 10^3 zoospores mL^{-1}) to three (for 10^4 zoospores mL^{-1}) orders of magnitude.

Environmental factors and pathogen abundance for environmental samples

During the sampling process, almost all the measured environmental factors in Haizhou Bay were dynamically changed, with significant differences determined in temperature, pH, salinity, DO, and concentrations of NO_2^--N, and SiO_3^{2-}-Si among months (Supplementary Table S3). Notably, December 2021 was significantly higher in temperature but significantly lower in salinity compared with January and February 2022 (Supplementary Table S3). On December 23, 2021, when red rot occurred, spatial comparison determined significantly lower DO at the uninfected S9 site compared with the infected two sub-sites (Supplementary Table S4). Although differences were not significant, the uninfected S9 site was determined to be higher in nutrients, such as NH_4^+-N, NO_2^--N, NO_3^--N, and PO_4^{3-}-P (Supplementary Table S4).

Both pathogens can be detected in Haizhou Bay during the sampling process (Fig. 4). Overall, *P. porphyrae* was more abundant than *P. chonricola*, and the abundance of *P. porphyrae* was less than 10^4 copies mL^{-1} compared to 10^3 copies mL^{-1} for *P. chondricola* within most of the

Table 2. Zoospore quantification using the present method

Pythium porphyrae		*Pythium chondricola*	
Zoospores mL^{-1}	Copies mL^{-1}[a]	Zoospores mL^{-1}	Copies mL^{-1}
1.4×10^6	$(2.34 \pm 0.24) \times 10^2$	-	-
1.4×10^5	$(1.41 \pm 0.01) \times 10^1$	-	-
1.4×10^4	$(5.86 \pm 0.35) \times 10^0$	1.5×10^4	$(3.49 \pm 0.16) \times 10^3$
1.4×10^3	$(1.58 \pm 0.03) \times 10^0$	1.5×10^3	$(2.63 \pm 0.33) \times 10^2$
1.4×10^2	$(4.62 \pm 0.82) \times 10^{-1}$	1.5×10^2	$(1.48 \pm 0.23) \times 10^1$
1.4×10^1	ND	1.5×10^1	$(1.51 \pm 0.15) \times 10^0$

ND, not detected.
[a]The determined abundance was shown as mean ± standard deviation (n = 4).

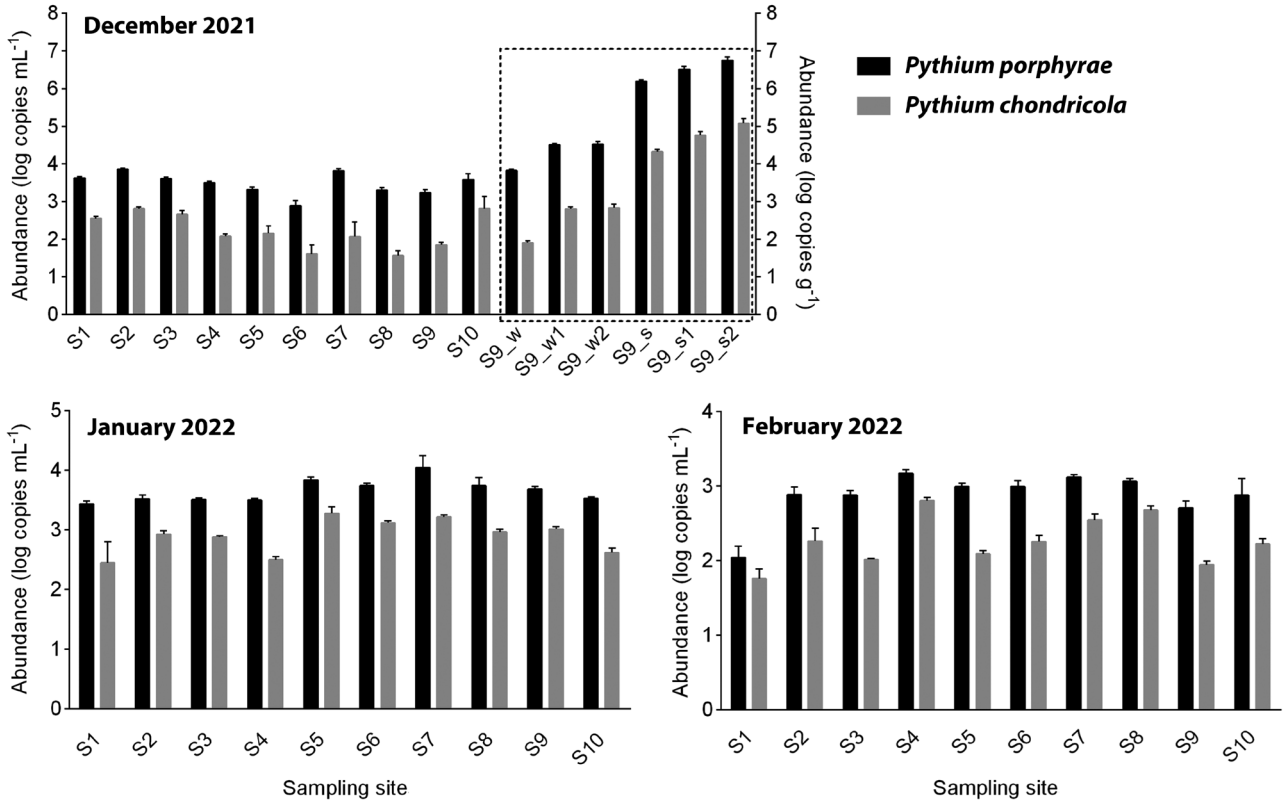

Fig. 4. Quantitative detection of *Pythium porphyrae* and *P. chondricola* in environmental samples in December 2021, January 2022, and February 2022. Error bars indicate standard deviations. Plots in the dotted box represent detected pathogen abundance when red rot disease occurred on December 23, 2021. Sample names with "w" indicate seawater samples, and those with "s" indicate sediment samples. For comparisons, the abundance of these samples was transformed to "copies g^{-1}" using an averaged seawater density (1.025 g mL^{-1}).

seawater samples (Supplementary Tables S5 & S6). For *P. porphyrae*, the abundance was determined to be (3.60 ± 2.08) × 10^3 copies mL^{-1} in December 2021, and increased to (5.08 ± 2.82) × 10^3 copies mL^{-1} in January 2022, and then decreased to (8.94 ± 3.95) × 10^2 copies mL^{-1} for the seawater in this bay. A similar pattern was observed for *P. chondricola*. The abundance was determined to be (2.82 ± 1.16) × 10^2 copies mL^{-1} in December 2021, increased to (9.54 ± 5.48) × 10^2 copies mL^{-1} in January 2022, and then decreased to (2.40 ± 1.91) × 10^2 copies mL^{-1}. When there was an occurrence of red rot disease on December 23, 2021, the two pathogens were significantly more abundant at infected sub-sites (i.e., S9-1 and S9-2) than the uninfected sub-site (S9) within both seawater ($p < 0.00001$, ANOVA with Tukey's *post-hoc* test) and sediment ($p < 0.01$, ANOVA with Tukey's *post-hoc* test) (Fig. 4, Supplementary Table S7). Besides, the two pathogens were significantly enriched in sediment (>10^6 copies g^{-1} for *P. porphyrae*, and >10^4 copies g^{-1} for *P. chondricola*) than seawater ($p < 0.0001$, unpaired t-test) (Fig. 4, Supplementary Table S7).

DISCUSSION

In China, the cultivation of *Pyropia* is usually carried out from November until the beginning of April next year, which contributed to a production worth more than US $1 billion (FAO, 2024). However, multiple lines of evidence have demonstrated that the occurrence of oomycete diseases (e.g., red rot disease, *Olpidiopsis* disease) can significantly reduce the yield and even lead to total crop failure in certain farms (Ding and Ma 2005, Yan et al. 2019). Unlike *Olpidiopsis* sp., the pathogens of red rot disease have been isolated in the aquaculture farms in China, and frequently identified as *P. porphyrae* and *P. chondricola* (Ding and Ma 2005, Qiu et al. 2019, Yan et al. 2019). Such observation has provided good opportunities for phylogeny or pathogenesis research, since related genomic and transcriptomic data have been reported for the two pathogens (Im et al. 2019, Tang et al. 2019, Nguyen et al. 2022).

Recently, some researchers argued that the current

genetic information is insufficient to distinguish *P. porphyrae* and *P. chondricola* as separate species (Diehl et al. 2017, Wen et al. 2023), though their *cox1* and *cox2* sequences varied as demonstrated in the present study (Supplementary Fig. S2). It is also noted that both the phylogenetic analysis and specificity tests demonstrated that the *Pythium* strains NBRC No. 33253 and No. 100633 were more affiliated with *P. chondricola*, which is different from the deposited name *P. porphyrae* in NBRC. Therefore, many more efforts are required to resolve the taxonomic information for these *Pythium* strains. Despite the controversy, the present phylogenetic analysis and amplification specificity tests, in addition to previously reported morphological and physiological differences (Lévesque and De Cock 2004), demonstrated that the pathogens are somewhat distinct. Therefore, based on current knowledge, the detection, prediction, and treatment for red rot disease are supposed to be performed separately regarding the pathogens. However, there are limited attempts to detect the two pathogens to know their distributions, and thus to predict and prevent red rot disease (Lee and Lee 2022).

In the present study, a quantitative method was established to detect the distributions of *P. porphyrae* and *P. chondricola* based on pathogen-specific PCR primers. Notably, an overlapping PCR was used to concatenate the pathogen-specific fragments of the two pathogens and construct an internal standard plasmid. Therefore, the established method requires one single standard plasmid to accomplish the quantification of the two pathogens, which provides convenience in comparing the abundance of the two pathogens in the same sample. In addition, it also facilitates the monitoring and comparison of the distributions of the two pathogens in different sea areas and at different time points.

To evaluate the current method, it is first used for quantifying the known numbers of zoospores in seawater. It is demonstrated that the method is capable of detecting approximately 100 and 10 zoospores mL^{-1} in a 200 mL solution for *P. porphyrae* and *P. chondricola*, respectively, which provides the capability to forecast disease occurrence. According to a previous report, there will be an interval of approximately three to four days prior to infection if 10 and 100 zoospores are presented in seawater (Park et al. 2006). When applied to environmental samples, the detected abundance of both pathogens significantly increased in both seawater and sediment when the sub-sites were infected by red rot disease, which further suggested an indication of disease occurrence. It is noted that the abundance of the pathogens was significantly higher in the marine sediment than in the seawater, no matter if there was disease occurrence or not. It was reported that *Pythium* pathogens can be present in seafloor sediment in culturing areas (Kawamura et al. 2005). Therefore, the bottom sediment potentially increases the transmission pathways of *Pythium* and increases the possibility of disease development (Ding and Ma 2005). On the other hand, *Pythium* zoospores, an important inoculum for disease occurrence and spread, may also be delivered through terrestrial runoff, making it a potential source to initiate red rot disease (Klochkova et al. 2017). Given five rivers flow into Haizhou Bay, the possibility that the pathogens may originate from land cannot be precluded since red rot disease has been reported in a coastal area in Haizhou Bay (Yan et al. 2019), which is adjacent to the current infected area. In such a context, long-term monitoring is warranted for the cultured areas and the surrounding environments, e.g., seawater, sediment, rivers, and canals. Besides, environmental parameters should also be included. Multiple lines of evidence have demonstrated that higher temperature and lower salinity are highly associated with disease occurrence (Ding and Ma 2005, Klochkova et al. 2017), which was also determined in December 2021 in the investigation when a red rot disease occurred.

It is noted that the determined copy number of *P. porphyrae* tended to be less than *P. chondricola* when compared to the same zoospore concentrations. Multiple lines of evidence demonstrated that longer amplicon length resulted in lower amplification efficiency, which in turn leads to underestimation of microbial abundance (Pionzio and McCord 2014, Debode et al. 2017). The determined amplification efficiency (Fig. 2) is consistent with this observation for that of *P. porphyrae* (E = 0.73) being lower than that of *P. chondricola* (E = 1.07). Therefore, certain optimization is supposed to be performed, and a shorter amplicon is supposed to be preferred. Besides, the detected abundance (i.e., copies mL^{-1}) for each pathogen was lower than zoospore concentrations in magnitudes. As such, more zoospores were supposed to be determined in seawater samples in Haizhou Bay, indicating more infections from December 2021 to February 2022. However, no disease was reported in the investigation except on December 23, 2021, when the copy numbers of *P. porphyrae* and *P. chondricola* were more than 10^4 copies mL^{-1} and 10^2 copies mL^{-1} in seawater, respectively. This might be attributed to plenty of dead zoospores or mycelium within the seawater. In such a context, quantification using such complicated environmental DNA might overestimate the number of infective zoospores.

Therefore, it might be useful to construct standard curves using known quantities of target DNA extracted from field-collected samples, which could provide a more realistic basis across the variable conditions encountered in field samples. On the other hand, long-term monitoring is also warranted during periods from *Pyropia* not under cultivation to cultivation, notably in combination with the onset and full-scale transmission of red rot disease. These works will be useful in establishing baseline data and threshold values to forecast disease. Previously, spatial comparisons have been performed and determined that local changes in reactive silicate and salinity in addition to planktonic and epiphytic microbiomes were associated with red rot disease, which might be useful for predicting disease (Yan et al. 2019). In the present study, the determined lower nutrient concentrations at infected sub-sites (NH_4^+-N, NO_2^--N, NO_3^--N, and PO_4^{3-}-P) might be responsible for pathogen infection by undermining host status and thus highlight the importance to perform the aforementioned monitoring.

Taken together, a qPCR method is established to quantitatively monitor two pathogens of red rot disease using pathogen-specific primers. The developed method is capable of detecting approximately 100 and 10 zoospores mL^{-1} using a 200 mL solution for *P. porphyrae* and *P. chondricola*, respectively. In Haizhou Bay, a significantly higher temperature and a significantly lower salinity were determined in December 2021 compared with January and February 2022. Although similar temporal patterns were determined from December 2021 to February 2022, *P. porphyrae* was determined to be more abundant than *P. chondricola*. Besides, significantly higher abundance of the two pathogens was detected in both seawater and sediment when there was an occurrence of red rot disease. In addition, there was a significant enrichment of the pathogens in the bottom sediment in the culturing area, which indicated a potential storage for pathogens. Although it requires further optimization, the present method shows a potential to forecast disease occurrence, which is of great significance to take in-time measures to prevent disease and thus avoid economic losses. Besides, more environmental samples including seawater and sediment are supposed to be collected to correlate pathogen abundance and disease occurrence, which is essential to forecast disease.

ACKNOWLEDGEMENTS

This work was funded by National Key Research and Development Program of China (2023YFD2400704), China Agriculture Research System of Ministry of Agriculture and Rural Affairs (CARS-50), and Key Scientific Research Project Universities and Colleges in Tianjin (2022ZD004).

CONFLICTS OF INTEREST

The authors declare that they have no potential conflicts of interest.

SUPPLEMENTARY MATERIALS

Supplementary Method S1. Phylogenetic analysis and primer design (https://www.e-algae.org).

Supplementary Table S1. Microbes used for the specificity test of the pathogen-specific primers (https://www.e-algae.org).

Supplementary Table S2. Coordinates of the sampling sites distributed in Haizhou Bay (https://www.e-algae.org).

Supplementary Table S3. Measurements of environmental parameters in Haizhou Bay (https://www.e-algae.org).

Supplementary Table S4. Comparison of environmental factors among sub-sites on December 23, 2021 (https://www.e-algae.org).

Supplementary Table S5. Quantification of *Pythium porphyrae* in Haizhou Bay using the present method (https://www.e-algae.org).

Supplementary Table S6. Quantification of *Pythium chondricola* in Haizhou Bay using the present method (https://www.e-algae.org).

Supplementary Table S7. Comparison of pathogen abundance in environmental samples on December 23, 2021 (https://www.e-algae.org).

Supplementary Fig. S1. Schematic of overlapping polymerase chain reaction (A) and the positions of primers in concatenated sequence (B) (https://www.e-algae.org).

Supplementary Fig. S2. Neighbor-joining phylogenetic analyses of *Pythium* isolates using the *cox*1 (A) and *cox*2 (B) regions (https://www.e-algae.org).

Supplementary Fig. S3. Amplification curves and melting curves (https://www.e-algae.org).

REFERENCES

Addepalli, M. K. & Fujita, Y. 2002. Regulatory role of external calcium on *Pythium porphyrae* (Oomycota) zoospore release, development and infection in causing red rot disease of *Porphyra yezoensis* (Rhodophyta). FEMS Microbiol. Lett. 211:253–257. doi.org/10.1111/j.1574-6968.2002.tb11233.x

Amano, H., Sakaguchi, K., Maegawa, M. & Noda, H. 1996. The use of a monoclonal antibody for the detection of fungal parasite, *Pythium* sp., the causative organism of red rot disease, in seawater from *Porphyra* cultivation farms. Fish. Sci. 62:556–560. doi.org/10.2331/fishsci.62.556

Amano, H., Suginaga, R., Arashima, K. & Noda, H. 1995. Immunological detection of the fungal parasite, *Pythium* sp.: the causative organism of red rot disease in *Porphyra yezoensis*. J. Appl. Phycol. 7:53–58. doi.org/10.1007/BF00003550

Behera, D. P., Ingle, K. N., Mathew, D. E., et al. 2022. Epiphytism, diseases and grazing in seaweed aquaculture: a comprehensive review. Rev. Aquac. 14:1345–1370. doi.org/10.1111/raq.12653

Debode, F., Marien, A., Janssen, É., Bragard, C. & Berben, G. 2017. The influence of amplicon length on real-time PCR results. Biotechnol. Agron. Soc. Environ. 21:3–11. doi.org/10.25518/1780-4507.13461

Diehl, N., Kim, G. H. & Zuccarello, G. C. 2017. A pathogen of New Zealand *Pyropia plicata* (Bangiales, Rhodophyta), *Pythium porphyrae* (Oomycota). Algae 32:29–39. doi.org/10.4490/algae.2017.32.2.25

Ding, H. & Ma, J. 2005. Simultaneous infection by red rot and chytrid diseases in *Porphyra yezoensis* Ueda. J. Appl. Phycol. 17:51–56. doi.org/10.1007/s10811-005-5523-6

FAO. 2024. Available from: https://www.fao.org/fishery/statistics-query/en/aquaculture/aquaculture_value. Accessed May 17, 2024.

Fujita, Y. & Zenitani, B. 1977. Studies on pathogenic *Pythium* of laver red rot in Ariake sea farm: IV. Serological differentiation of pathogenic *Pythium* strain. Nippon Suisan Gakkaishi 43:1313–1318 (in Japanese). doi.org/10.2331/suisan.43.1313

Gachon, C. M. M., Sime-Ngando, T., Strittmatter, M., Chambouvet, A. & Kim, G. H. 2010. Algal diseases: spotlight on a black box. Trends Plant Sci. 15:633–640. doi.org/10.1016/j.tplants.2010.08.005

Heckman, K. L. & Pease, L. R. 2007. Gene splicing and mutagenesis by PCR-driven overlap extension. Nat. Protoc. 2:924–932. doi.org/10.1038/nprot.2007.132

Im, S. H., Klochkova, T. A., Lee, D. J., Gachon, C. M. M. & Kim, G. H. 2019. Genetic toolkits of the red alga *Pyropia tenera* against the three most common diseases in *Pyropia* farms. J. Phycol. 55:801–815. doi.org/10.1111/jpy.12857

Kawamura, Y., Yokoo, K., Tojo, M. & Hishiike, M. 2005. Distribution of *Pythium porphyrae*, the causal agent of red rot disease of *Porphyrae* spp., in the Ariake Sea, Japan. Plant Dis. 89:1041–1047. doi.org/10.1094/pd-89-1041

Kazama, F. Y. 1979. *Pythium* 'red rot disease' of *Porphyra*. Experientia 35:443–444. doi.org/10.1007/BF01922695

Kim, G. H., Moon, K.-H., Kim, J.-Y., Shim, J. & Klochkova, T. A. 2014. A revaluation of algal diseases in Korean *Pyropia* (*Porphyra*) sea farms and their economic impact. Algae 29:249–265. doi.org/10.4490/algae.2014.29.4.249

Klochkova, T. A., Jung, S. & Kim, G. H. 2017. Host range and salinity tolerance of *Pythium porphyrae* may indicate its terrestrial origin. J. Appl. Phycol. 29:371–379. doi.org/10.1007/s10811-016-0947-8

Lai, P. Y. 2009. Investigation and countermeasure of rot disease of *Porphyra haitanensis* in Fuding City in autumn 2008. Mod. Fish. Inf. 24:6–9 (in Chinese).

Lee, S. J., Hwang, M. S., Park, M. A., et al. 2015. Molecular identification of the algal pathogen *Pythium chondricola* (*Oomycetes*) from *Pyropia yezoensis* (Rhodophyta) using ITS and cox1 markers. Algae 30:217–222. doi.org/10.4490/algae.2015.30.3.217

Lee, S. J. & Lee, S.-R. 2022. Rapid detection of red rot disease pathogens (*Pythium chondricola* and *P. porphyrae*) in *Pyropia yezoensis* (Rhodophyta) with PCR-RFLP. Plant Dis. 106:30–33. doi.org/10.1094/PDIS-07-21-1494-SC

Lévesque, C. A. & De Cock, A. W. A. M. 2004. Molecular phylogeny and taxonomy of the genus *Pythium*. Mycol. Res. 108:1363–1383. doi.org/10.1017/S0953756204001431

Mo, Z., Li, S., Kong, F., Tang, X. & Mao, Y. 2016. Characterization of a novel fungal disease that infects the gametophyte of *Pyropia yezoensis* (Bangiales, Rhodophyta). J. Appl. Phycol. 28:395–404. doi.org/10.1007/s10811-015-0539-z

Nguyen, H. D. T., Dodge, A., Dadej, K., et al. 2022. Whole genome sequencing and phylogenomic analysis show support for the splitting of genus *Pythium*. Mycologia 114:501–515. doi.org/10.1080/00275514.2022.2045116

Park, C. S., Kakinuma, M. & Amano, H. 2001. Detection of the red rot disease fungi *Pythium* spp. by polymerase chain reaction. Fish. Sci. 67:197–199. doi.org/10.1046/j.1444-2906.2001.00224.x

Park, C. S., Kakinuma, M. & Amano, H. 2006. Forecasting infections of the red rot disease on *Porphyra yezoensis* Ueda (Rhodophyta) cultivation farms. J. Appl. Phycol. 18:295–299. doi.org/10.1007/s10811-006-9031-0

Pionzio, A. M. & McCord, B. R. 2014. The effect of internal control sequence and length on the response to PCR in-

hibition in real-time PCR quantitation. Forensic Sci. Int. Genet. 9:55–60. doi.org/10.1016/j.fsigen.2013.10.010

Qiu, L., Mao, Y., Tang, L., Tang, X. & Mo, Z. 2019. Characterization of *Pythium chondricola* associated with red rot disease of *Pyropia yezoensis* (Ueda) (Bangiales, Rhodophyta) from Lianyungang, China. J. Oceanol. Limnol. 37:1102–1112. doi.org/10.1007/s00343-019-8075-3

Satoshi, F. 2016. Development of a quantitative detection technique for the pathogen zoospores of red rot disease. Bull. Fukuoka Fish. Mar. Technol. Res. Cent. 26:93–96 (in Japanese).

Takahashi, M., Ichitani, T. & Sasaki, M. 1977. *Pythium porphyrae* Takahashi et Sasaki, sp. nov. causing red rot of marine red algae *Porphyra* spp. Trans. Mycol. Soc. Jpn. 18:279–285 (in Japanese).

Tang, L., Qiu, L., Liu, C., et al. 2019. Transcriptomic insights into innate immunity responding to red rot disease in red alga *Pyropia yezoensis*. Int. J. Mol. Sci. 20:5970. doi.org/10.3390/ijms20235970

Vandesompele, J., De Preter, K., Pattyn, F., et al. 2002. Accurate normalization of real-time quantitative RT-PCR data by geometric averaging of multiple internal control genes. Genome Biol. 3:research0034.1. doi.org/10.1186/gb-2002-3-7-research0034

Ward, G. M., Faisan, J. P. Jr., Cottier-Cook, E. J., et al. 2019. A review of reported seaweed diseases and pests in aquaculture in Asia. J. World Aquacult. Soc. 51:815–828. doi.org/10.1111/jwas.12649

Wen, X., Zuccarello, G. C., Klochkova, T. A. & Kim, G. H. 2023. Oomycete pathogens, red algal defense mechanisms and control measures. Algae 38:203–215. doi.org/10.4490/algae.2023.38.12.13

Weng, P., Yang, H., Mo, Z., et al. 2024. Application and evaluation of probiotics against red rot disease in *Pyropia*. Aquaculture 578:740050. doi.org/10.1016/j.aquaculture.2023.740050

Yan, Y.-W., Yang, H.-C., Tang, L., Li, J., Mao, Y.-X. & Mo, Z.-L. 2019. Compositional shifts of bacterial communities associated with *Pyropia yezoensis* and surrounding seawater co-occurring with red rot disease. Front. Microbiol. 10:1666. doi.org/10.3389/fmicb.2019.01666

Yang, L.-E., Deng, Y.-Y., Xu, G.-P., Russell, S., Lu Q.-Q. & Brodie, J. 2020. Redefining *Pyropia* (Bangiales, Rhodophyta): four new genera, resurrection of *Porphyrella* and description of *Calidia pseudolobata* sp. nov. from China. J. Phycol. 56:862–879. doi.org/10.1111/jpy.12992